Zhang *et al. Chem. Biol. Technol. Agric.* (2024) 11:106
https://doi.org/10.1186/s40538-024-00630-9

Chemical and Biological Technologies in Agriculture

RESEARCH

Open Access

The synergistic effect of biosynthesized CuONPs and phage (φPB2) as a novel approach for controlling *Ralstonia solanacearum*

Hongbao Zhang[1†], Liuti Cai[2†], Kai Yuan[3], Zhongwei Liu[1], Maoyang Ran[1], Siang Chen[3], Wu Cai[4], Cheng Rao[4], Lin Cai[1*] and Dong Zhou[3*]

Abstract

Background As a vital soil-borne pathogenic bacterium, *Ralstonia solanacearum* can cause wilt disease in multiple *Solanaceae* plants. Several phages, such as φPB2, could infect *R. solanacearum* acting as a potential biological control agent in soil. In addition, some nanoparticles, especially copper preparation, also showed high toxicity on *R. solanacearum* with low toxicity on plant. However, whether they can be administered in combination and how effective they are in inhibiting the plant disease caused by *R. solanacearum* is known very little.

Results In this work, the characterization of CuONPs using scanning electron microscope, transmission electron microscope, X-ray photoelectron spectroscopy, Fourier transform infrared spectroscopy, and X-ray diffraction ascertained the presence of CuONPs which were nanometer particle of 83 nm. Then it was found that combined application of CuONPs with phage (φPB2) was superior to that of φPB2 or CuONPs alone in controlling tobacco bacterial wilt, with the CuONPs (250 mg/mL) and phage (10^6 PFU/mL) ratio being the best, at 79.1%. The combination of CuONPs and φPB2 also showed no obvious toxicity on tobacco growth than control like single application of CuONPs or φPB2. Furthermore, the transcriptome changes of *R. solanacearum* analysis indicated that the combination application and single allocation of CuONPs could inhibit "biofilm formation", molecular function, biological processes, cellular components, metabolic process, and so on. In addition, the combination application showed higher inhibition of motility and biofilm, and better enhancement of cell membrane permeability, protein leakage, MDA concentration, and enzyme activity of their respiratory chain dehydrogenase than single application of CuONPs or phage (φPB2). Transcriptomes analysis also supported that the addition of φPB2 enhanced the toxicity of CuONPs by influencing the ABC transporters and quorum sensing, metabolic processes, and cellular biosynthetic processes of *R. solanacearum*.

Conclusion In total, our work not only proposed a novel way to increase the bactericidal effect of nanomaterials by adding phage, but also discovered the influence, synergistic effects, and mechanisms, which is useful to design novel way to combat phytopathogenic bacteria in the complicated environment.

Keywords CuONPs + phage, Tobacco bacterial wilt, Synergistic effect, Antibacterial mechanism, Transcriptome analysis

†Hongbao Zhang and Liuti Cai have contributed equally to this work.

*Correspondence:
Lin Cai
lincai@gzu.edu.cn
Dong Zhou
1456911243@qq.com
Full list of author information is available at the end of the article

Graphical abstract

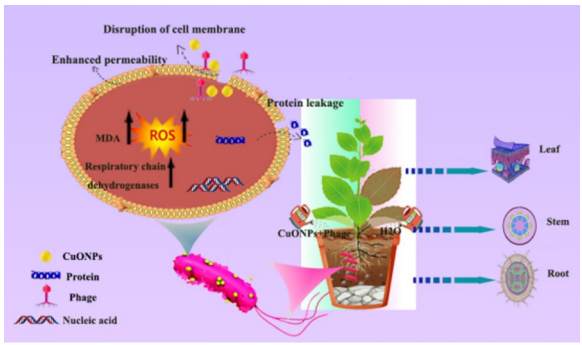

Introduction

The increasing global population and food demand have put tremendous pressure on the agricultural sector [1]. At the same time, biological stress caused by plant diseases seriously affects crop yield and quality [2]. Crop failure due to pathogen infection is a widespread problem in agriculture. Each year, more than 30% of crop losses are caused by plant diseases [3, 4]. Among these diseases, *R. solanacearum* is a vital soil-borne pathogenic bacterium and one of the top ten destructive plant pathogens worldwide [5, 6]. It is the pathogenic factor of bacterial wilt in more than 450 plants, including important agricultural crops such as tobacco, tomato, potato, mulberry, and peanut [7]. To control it, chemical control, physical control, and biological control are often used for crop protection [8, 9]. In addition, the powerful ability to cause disease of *R. solanacearum* and its increasing new host range make it a great threat to agricultural crops [10]. Therefore, it is urgent to develop an effective strategy to control bacterial wilt in agriculture.

Numerous biological control strategies have been implemented to resist bacterial disease in an environmentally friendly and highly pathogen-specific manner [11]. The biological control of bacterial wilt primarily focuses on the use of antagonistic microorganisms, usually nontoxic pathogenic mutants and strains of other bacterial species, as well as some fungi and phage [12, 13]. In recent years, phage have been reported as a promising strategy to control plant bacterial diseases [14, 15]. Phage can restrict the pathogenic virulence by decreasing the number of pathogenic bacteria and the expression of bacterial toxicity genes. Some research shows the potential use of phage to control bacterial wilt, which could significantly increase tobacco plant yields [16, 17]. Recent research is directed toward supporting the phage with other substances to reach a synergy that would decrease the incidence of phage resistance [18, 19]. Studies have shown that phages combined with the natural product of green synthesis, AgNPs, will improve their biological control efficiency and reduce bacterial resistance [14]. Since the beginning of 2005, nanomaterials have been extensively and intensively studied with a view to their use in medical and pharmaceutical applications [20]. Nanomaterials are characterized by showing a size of 100nm or less on at least one side and include metal, semiconductor, polymer, or carbon-based materials. The antimicrobial activity of nanomaterials results from the biophysical interactions that occur between their nanoparticles and bacteria, including cell absorption and nanoparticle aggregation, leading to membrane damage and toxicity [21]. Nanomaterials have recently been applied to the production of antimicrobial drugs due to their high antimicrobial rates against both Gram-negative and Gram-positive bacteria [22, 23]. Their unique antibacterial mechanism also makes it difficult for bacteria to develop targeted drug resistance [24, 25]. The research demonstrates that CuONPs possess broad-spectrum antibacterial properties. These nanoparticles enter cells and bind to essential enzymes, impeding cell functionality and causing cell death [26], and that some metal nanoparticles, such as silver and magnesium oxide, are conducive to the control of bacterial wilt because of their role in facilitating the production of reactive oxygen species (ROS) and promoting oxidative stress [27, 28]. On the other hand, there is a need for synthetic techniques that are organism, environmentally friendly, cost-effective, and easily implemented because there are increasingly popular concerns related to the environment and safety [29].

Here, the aim of this study was to evaluate whether phages can enhance the antibacterial activity of CuONPs synthesized from orange peel against *R. solanacearum*,

and to explore the mechanism of their interaction with *R. solanacearum* cells. In this process, CuONPs and phage produce a large amount of ROS through direct interaction with pathogenic bacteria. As a result, pathogens are subjected to oxidative stress, and further hinder various metabolic pathways, destroy membrane structure, and enhance membrane permeability. Intracellular material leakage inhibits vegetative growth and reproductive growth or cause them to die. Phage combined with CuONPs is an effective antibacterial strategy against bacterial wilt, and we aim to investigate the underlying mechanism of this disease inhibition.

Materials and methods

Chemicals and materials

The citrus peel required for the test was obtained from citrus fruits purchased by Walmart Supermarket in Huaxi District, Guiyang City. The reagents used include copper nitrate tetrahydrate ((CuNO3)2·5H2O; Aladdin), sodium hydroxide (NaOH; Macklin), acetone (Aladdin), and distilled water. All reagents were analytically pure. The strain of *R. solanacearum* (Biovar 3, phylotype I) was isolated and purified from strains collected in Guiyang; the phage (ϕPB2, *Caudovirales, Podoviridae*) of *R. solanacearum* was provided from Liuti Cai, a researcher of Guizhou Tobacco Research Institute [30].

Biosynthesis of CuONPs

The orange peel was dried in a 70 ℃ oven until it reached a constant weight. After drying, it was ground into a fine powder. The fine powder was then dissolved in distilled water using magnetic stirring for 3 h. The resulting mixture was filtered and refrigerated for future use. Next, a conical flask was used to heat copper nitrate (0.01 M) to 90 ℃ with brisk stirring. Then 20 mL of prepared orange peel extract were added to the conical flask. This addition caused a light color change from blue to green. To achieve a dark blue and bright red and yellow solution, approximately 5 mL of 1 mol/L NaOH was added to each flask. The flasks were then stirred for 4 h. After the stirring process, the mixture was cooled to room temperature and centrifuged at 6000 rpm. This centrifugation process was repeated several times, with each repetition involving washing the sediment with distilled water. The resulting washed samples, which took on a yellow–brown color, were collected and reacted in a muffle furnace at 200 °C to produce black solid particles [31].

Antibacterial effect of CuONPs on *R. solanacearum*

The 500 μL bacterial subtilis solution and 500 μL CuONPs cultured overnight were added into 1.5 mL centrifuge tube to make the final concentrations of CuONPs 0, 62.5, 125, 250, and 500 mg/L, respectively. The samples were mixed and incubated in a 28 ℃ constant-temperature oscillation incubator for some time, and then coated. The culture dish was incubated in a 28 ℃ constant-temperature incubator for 2 days, and then counted [32].

In this study [33], the growth of *R. solanacearum* was measured using ultraviolet (UV) spectrophotometer over a period of 24 h using OD_{600} as measurement index. Fresh *R. solanacearum* (OD_{600} = 0.1) was collected and added to LB medium to form a suspension. Then CuONPs or 100 μL phage + CuONPs were added to make final concentrations, respectively, of 0, 62.5, 125, and 250 mg/L. Subsequently, the bacterial solution was incubated at 28 °C. The bacterial solution was removed every 4 h, and the absorbance values were measured on an UV spectrophotometer. Each treatment was repeated at least three times.

Antibacterial effect of phage on *R. solanacearum*

The concentrations of 500 μL fresh bacterial solution (OD_{600}=1.0) and bacteriophage solution (10^3, 10^4, 10^5, 10^6, 10^7 PFU/mL) were added into 1.5 mL centrifuge tube, and then CuONPs was added to make the concentration 250 mg/L. After mixing, the sample was placed in a constant-temperature oscillating incubator for 1 h, and 100 μL was coated on a LB petri dish at 28 ℃ for 2 days culturing, and then the number of colonies was calculated [34].

Extracellular membrane permeability assay

N-Phenyl-1-naphthylamine (NPN) is a hydrophobic fluorescent agent, which can only emit weak fluorescence in aqueous solution [35]. But when it enters hydrophobic media, such as cells, it will emit strong fluorescence. For normal and complete outer membrane, NPN is usually plugged. If the outer membrane structure is damaged, the permeability inside and outside the cell will change, then NPN can enter cells and emit fluorescence. Phage or CuONPs was put into a centrifuge tube containing *R. solanacearum*, then it was put still at 28 ℃ for incubation for 1 h, whereupon sub-packed on black 96-well plate, a pipette gun was used to add NPN prepared from acetone into the plate, so that the concentration of NPN is 10 μM. At once, a blank control without bacteria was set, and the fluorescence value was measured by the multimode microplate reader (Infinite M1000 PRO, Tecan, Austria). During measurement, the excitation wavelength was set to 350 nm and the emission wavelength was set to 420 nm.

Intracellular ROS (•OH) levels

To assess the effect of CuONPs treatment on the intracellular ROS level of *R. solanacearum*, DCFH-DA was used to detect the production of •OH [36]. The *R.*

solanacearum was cultured to the late logarithmic phase and washed twice with PBS. Under dark conditions, the cells at 10 μL were incubate in DCFH-DA for 20 min, mixed upside down every 3–5 min, and then washed it with PBS three times to remove the redundant probe. CK group was the control without nanomaterials. After mixing, the sample was placed at 28 ℃ for incubation for 1 h. Then 200 μL sample was pipetted into a black 96-well plate, and fluorescence intensity was measured with the multimode microplate reader (Infinite M1000 PRO, Tecan, Austria). The excitation wavelength was 488 nm and the emission wavelength was 525 nm.

Lipid peroxidation analysis

Reactive oxygen free radicals are one of the causes of bacterial cell membrane damage. The content of malondialdehyde (MDA) in the bacterial solution treated with composite antibacterial materials was determined by 2-thiobarbituric acid method, and the degree of bacterial lipid peroxidation was judged by this method, and the damage of ROS free radical to bacteria was further evaluated [37]. The specific detection method is as follows: first, add 1 mL of bacterial solution cultured to logarithmic growth stage into a centrifuge tube with 9 mL of deionized water, then augment 0.05 g of antibacterial material, and place it on a shaker for 20 min of reaction. Second, after the shaking is over, take 5 mL of the solution after shaking into the test tube, add 5 mL of 2-thiobarbituric acid solution containing 0.5% (weight concentration) and 5 mL of trichloroacetic acid solution containing 5% (volume concentration), heat it in a boiling water bath for 15 min, cool it in 30 ℃ water, and then centrifuge it at 8000 r/min for 10 min. Finally, take 3 mL of the supernatant to measure the absorbance value at 532 nm (where the colored substance formed by malondialdehyde and TBA has the maximum absorption) and 600 nm wavelength, and calculate the content of malondialdehyde using the following formula.

$$\text{Malondialdehyde content}\left(\text{nmol}\cdot\text{g}^{-1}\right) = (\text{A532}-\text{A600})\times\text{T}\times\text{v}/(\text{c}\times 0.155\times\text{m}),$$

where A532 and A600 are absorbance values at 532 nm and 600 nm, T is the total amount of solution during the reaction, V is the total amount of extract, C is the total amount of extract during the determination, m is the total amount of the material, and 0.155 is the molar absorbance of MDA.

Analysis of cell respiratory chain dehydrogenase

The detection method is as follows [38]: above all, *R. solanacearum* was cultivated to OD600=1.0. Subsequently, 0.05 g of different antibacterial materials was weighed and added to 8 mL of bacterial solution, and placed on a thermostatic shaking table for 1 h (temperature 28 ℃, speed 200 r/min). The mixture was centrifuged at 8000 r/min for 10 min, the supernatant was removed, washed with PBS buffer solution twice, and diluted to 8 mL with PBS. Then 500 μL of iodonitrotetrazolium chloride (INT) solution with a mass fraction of 0.5% was added into the centrifuge tube and vibrated for 1 h (temperature 28 ℃, speed 200 r/min) on a thermostatic shaking table. At the end of oscillation, 450 μL of formaldehyde solution was shaken for 20 min to terminate the reaction. Finally, it was centrifuged at a speed of 8000 r/min for 10 min, the supernatant was removed, the bacteria was collected, 3 mL of acetone and ethanol mixed solution (volume ratio 1:1) was added and shaken on a shaking table for 30 min, the insoluble reaction product nitro tetrazolium formamide (INF) was extracted, the supernatant was centrifuged, and the absorbance was measured at a wavelength of 490 nm, so as to compare the activity of bacterial respiratory chain dehydrogenase after treatment with different materials. The live bacteria without adding materials was selected for the control experiment, as the control (+), and completely inactivated bacteria after boiling for 20 min, was selected as the control (-).

Biofilm suppression assay

On the basis of previous studies, the biofilm formation test for *R. solanacearum* was slightly modified [39]. Briefly, using crystal violet in 96-well polystyrene microtiter plates, 1 μL of the fresh bacterial suspension (OD600 = 1.0) was added to 199 μL of the B medium with CuONPs or a mixture of phage and CuONPs was added to a final concentration of 0, 62.5, 125, or 250 mg/L, and the suspension was incubated for 24 h at 28 °C without shaking to form a biofilm. After the supernatant was discarded, crystal violet was added to the wells for staining. Ethanol (95%) was used to adsorb the excess crystal violet from the biofilm. The experiments were conducted while measuring the absorbance at 488 nm. Each experiment was repeated a minimum of three times.

Swimming and twitching motility assay

The effects of CuONPs or a mixture of phage and CuONPs on the twitching and swimming movement of *R. solanacearum* in the culture dish were studied to measure motility inhibition [40]. To observe the motility of bacterial cells after treatment with the CuONPs or CuONPs+ϕPB2, *R. solanacearum* cells were grown in a semisolid medium containing different concentrations of CuONPs (0, 62.5 mg/ L, 62.5 mg/ L+ϕPB2, 250 mg/L, 250 mg/L+ϕPB2). The 0.3% agar CPG medium was used for swimming assays, and 1.6% agar was used for the twitching motility test. First, the medium was

sterilized in an autoclave at 121 ℃ for 20 min, and 15 mL of CuONPs containing agar medium was poured into sterile Petri dishes (polystyrene, 90 mm diameter). Then bacterial suspensions were adjusted to 10^8 CFU mL^{-1}, and 100 µL portions were dropped in the middle of the prepared culture plates. Then the plates were placed horizontally in an incubator at 28 ℃ for 72 h. This procedure was carefully conducted to avoid disturbing the semisolid medium. All treatments were tested in triplicate. Swarming diameters and twitching were used as a measure of motility and were calculated as follows:

$$\text{Motility diameter} = \text{measured diameter (mm)} - \text{initial inoculation diameter}$$

Leakage of proteins

Protein leakage by the bacterial cells under the effect of nanoparticles was studied by Bradford assay [41]. Protein leakage is a cause of bacterial death, so 2,4-dinitrophenylhydrazine colorimetry was used to evaluate the leakage of bacterial protein. The detection method is as follows: first, a bacterial solution cultured to the logarithmic growth stage was centrifuged at 8000 r/min for 10 min at 4 ℃. The supernatant was collected, 20% glacial trichloroacetic acid solution was added, and the mixture was stored at − 20 ℃ for 1 h. After centrifuging the solution again, 0.4 mL of 2,4-dinitrophenyl hydrazine solution was added, and the solution was incubated in the dark for 1 h. After centrifugation, 10% glacial trichloroacetic acid solution was added for centrifugation, the supernatant was discarded, the precipitate was washed with ethanol–ethyl acetate (1:1), and extraction was performed with 10% glacial trichloroacetic acid solution. Finally, the residue was dissolved in 6 mol/L guanidine hydrochloride, incubated on a constant-temperature shaker at 28 ℃ for 10 min, and centrifuged at 8000 r/min for 5 min, and the supernatant was taken to measure the absorbance value at 370 nm.

The effect of different treatments on bacterial wilt and the impact of plant agronomic traits

Dozens of uniform tobacco seedlings were prepared for greenhouse experiments after 30 days of growth until the development of the fourth leaf [28, 42]. Tobacco seeds were sown in plastic pots (6.5 cm × 6.5 cm) filled with a peat substrate and placed in a manual climatic incubator at 28 ℃ with a light density of approximately 110 mmol m^{-2} s^{-1} and a light/dark photoperiod of 14 h/10 h. Then the tobacco plants were inoculated with *R. solanacearum*. The experiments included four groups (CK, ϕPB2, 250 mg/L CuONPs, 250 mg/L CuONPs + ϕPB2) and were conducted by the post-treatment method. In other words, 10 mL of *R. solanacearum* at OD_{600} = 0.5 (5×10^8 CFU mL^{-1}) was applied via non-injured root inoculation to the plant [43]. Twenty-four hours later, 10 mL suspensions for the four groups (CK, ϕPB2, 250 mg/L CuONPs, 250 mg/L CuONPs + ϕPB2) were applied by root drenching. We established four treatments, each consisting of five plants, and each treatment was repeated three times. Deionized water was used as a control group. All inoculated tobacco seedlings were incubated in the growth chamber at 28 ℃ under the same culture conditions and watered once every 2 days. After approximately 7 days of growth, bacterial wilt disease symptoms appeared. Then the disease occurrence in the tobacco seedlings and the disease index were investigated at 30 days. The bacterial wilt disease classification of the tobacco plants in the laboratory was evaluated and recorded according to the "Protocols of Disease Investigation and Classification". Disease indexes were calculated using the following equation [28]:

$$\text{Disease/index} = \sum (\text{ni} \times \text{vi})/\text{N} \times 4 \times 100,$$

where ni = number of diseased plants with the respective disease grade, vi= disease grade, N = total number of plants in each treatment, and 4 = the highest disease grade.

RNA extraction and sequencing

The samples were collected and quickly frozen in liquid nitrogen [42, 44]. Total RNA was isolated by TRIzol (Invitrogen, USA) according to the manufacturer's instructions. After genomic DNA was removed with DNase I (TaKaRa, Japan), the amount of RNA was assessed by agarose gel electrophoresis, a Nano Drop 2000 spectrophotometer (Thermo Scientific, United States), and an Agilent 2100 bioanalyzer (Agilent Technologies, United States). Only high-quality RNA samples (OD260/280=1.8~2.0, OD260/230≥2.0, RIN≥6.5, 28S:18S≥1.0, ≥100 ng/µL, ≥2 µg) were used to construct sequencing libraries. RNA purification, reverse transcription, library construction, and sequencing were performed according to the manufacturer's instructions (Illumina, San Diego, CA) as previously described [43]. After quantification by TBS380, a paired-end RNA-seq sequencing library was sequenced with an Illumina Nova Seq 6000 sequencer (2 × 150 bp read length). The sequence processing, base-calling, and quality value calculations of original images were performed using the Illumina GA Pipeline, in which 150 bp paired-end reads were obtained. A Perl program was written to select clean reads by removing low-quality sequences, reads with more than 5% N bases (unknown bases) and reads containing adaptor sequences.

Data analysis

The data generated from the Illumina platform were used for bioinformatics analysis [42, 45]. All analyses were performed using the I-Sanger Cloud Platform (www.i-sanger.com) as previously described [41], which was supported by Shanghai Majorbio Biopharm Biotechnology Co., Ltd. (Shanghai, China). Briefly, the raw paired-end reads from bacteria were trimmed by fast (https://github.com/OpenGene/fastp) with default parameters. High-quality reads in each sample were aligned to the genome (GCF_021117135.1) by Bowtie2 [45]. Ten thousand raw reads in each sample were randomly selected and aligned to the Rfam database (http://rfam.xfam.org/) with the blast method, and rRNA contamination was represented by this estimated percentage of rRNA in each sample. Gene and isoform abundances were quantified from single-end or paired-end RNA-Seq data using RSEM [46]. RSEM computes maximum likelihood abundance estimates using the expectation maximization (EM) algorithm for its statistical model, including the modeling of paired-end (PE) and variable-length reads, fragment length distributions, and quality scores, to determine which transcripts are isoforms of the same gene. TPM represents transcript per million mapped reads and is used to calculate expression levels. DESeq2 was used to calculate bacterial gene expression [44]. The criteria of false discovery rate (FDR) < 0.01 and fold changes <0.5 or >2.0 (< −1 or >1 in log2 ratio value) were used to identify the differentially expressed genes (DEGs). FDR correction was calculated by BH (multiple hypothesis test method). Functional classification was defined using Gene Ontology (GO) terms, which provide a wide range of functional classifications for genes and help us to understand the distribution of gene functions. Goatools was used to identify statistically significantly enriched GO terms using Fisher's exact test. Kyoto Encyclopedia of Genes and Genomes (KEGG) is a database for advanced functions and utilities of biological systems. KOBAS 2.0 was used to identify statistically significantly enriched pathways using Fisher's exact test. FDR < 0.05 was used as a cutoff for enrichment analysis of GO and KEGG [47].

Experimental results were statistically analyzed by SPSS software (version 22.0, IBM Corp.), and one-way analysis of variance (ANOVA) was applied to determine significant differences at a significance level of $p < 0.05$. The data were reported as the means of three replicates ± standard deviation (SD).

Results

Characterization of CuONPs

In this study, orange peel was used as raw material to synthesize nanomaterials (Fig. 1A). X-ray photoelectron spectroscopy was utilized to analyze the surface chemical properties of CuONPs generated via biotechnology. It presents three prominent sharp peaks of CuONPs at 934.08 eV, 530.08 eV, and 285.08 eV due to the copper photoelectron peak Cu2p. These peaks strongly indicate the existence of the spin orbit component CuO. In the photoelectron analysis of the surface details of CuONPs, Cu, O, and C are primarily present (Fig. 1B). Fourier transform infrared spectroscopy (FTIR) was conducted to identify the groups of CuONPs, and the O–H, C–H, C–OH, O–C O, C–C, and C –O groups were observed on their surface. More specifically, the absorption bands of O–H stretching vibrations appeared at 3440 cm^{-1}, while the C–O and C–C stretching vibrations were observed at 1820 cm^{-1}. Peaks at 1460 cm^{-1} and 1180 cm^{-1} were associated with C–H bending vibrations and C–O bending vibrations, respectively (Fig. 1C). The weak bands at 706 cm^{-1} could be attributed to the presence of metal oxide [48]. X-ray diffraction (XRD) was employed to identify the phase composition and structure of the synthesized CuONPs accurately. The peaks corresponding to 2θ values of 32.18°, 35.23°, 38.28°, 48.24°, 46.87°, 53.03°, 57.99°, 61.21°, 65.99°, 72.16°, and 74.64° correlate to (−111), (002), (111), (−202), (−113), (−311), (113), (311), and (004), respectively, indicating that the material is polycrystalline and consistent with the joint committee on powder diffraction standards (JCPDS) numbers 45-0937(Fig. 1D), and similar reports of this result have been found in the literature [49]. The morphology of phage particles was determined using transmission electron microscope (TEM) exactly as previously described following staining with 2% phosphotungstic acid (Fig. 1E). Scanning electron microscope (SEM) was used to confirm the morphology of the synthesized CuONPs (Fig. 1F). The image clearly demonstrates that the particles are regular. TEM image demonstrates a spherical shape and the size estimation that the average size was 83 nm (Fig. 1G), which is bigger in size than previous reported [50]. This result indicates the successful synthesis of high-purity CuONPs (Figs. 1H, I).

Antibacterial activity of CuONPs + phage (φPB2)

The antibacterial effect of CuONPs on *R. solanacearum* was assessed through plate counting method at various concentrations. A notable trend emerged, showing a decrease in bacterial survival rate with increasing CuONPs concentration, with the most potent antibacterial impact observed at the concentration of 250 mg/mL (Fig. 2A, B). Concurrently, at 250 mg/mL of CuONPs, the inhibitory effect of phage exhibited a positive correlation with varying concentrations until it plateaued when the phage concentration reached 10^6 PFU/mL (Fig. 2C, D). Visibly, untreated *R. solanacearum* cells displayed a

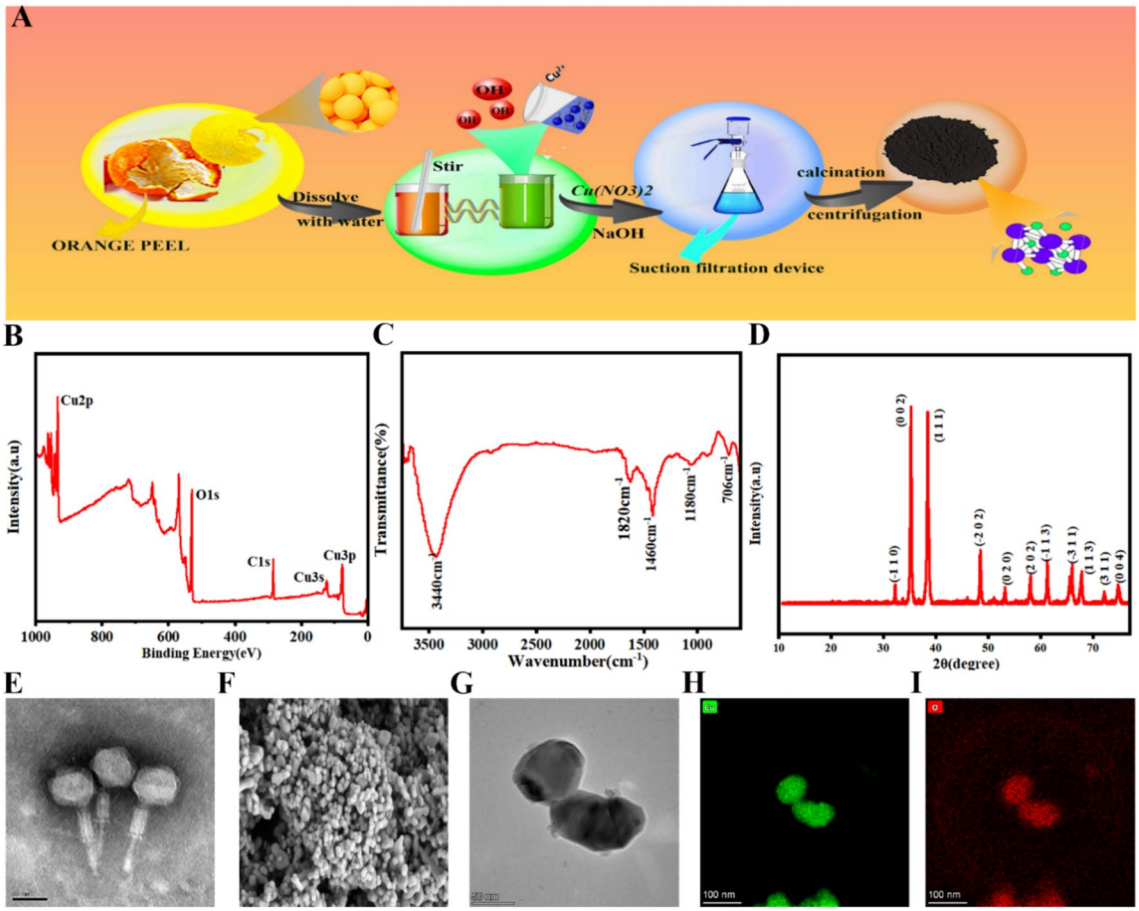

Fig. 1 Synthesis and characterization of CuONPs. **A** Organism synthesis process of CuONPs. **B** XPS of CuONPs, **C** FTIR of CuONPs. **D** XRD of CuONPs. **E** TEM of phage. **F** SEM of CuONPs. **G** TEM of CuONPs. **H**, **I** Energy spectrum distribution

smooth surface and maintained morphological integrity, unlike the treated cells in exponential growth stage. Following exposure to CuONPs + ϕPB2 at a concentration of 250 mg/L, drastic damage to bacterial morphology was noted, with noticeable cell deformation and wrinkling within the visual field. In contrast, the treatment with CuONPs at 250 mg/L resulted in roughened cell membranes, with only a few cells exhibiting hollow and twisted characteristics (Fig. 2E, F). The bacteriostatic effects of phages and CuONPs on bacteria are described in Fig. 2G. In addition, the extent of bacterial growth was analyzed by observing the 22-h growth curve, revealing a decline in bacterial proliferation as the concentrations of CuONPs and CuONPs + ϕPB2 increased. This decline indicated an augmented antibacterial efficacy with higher treatment concentrations. Notably, at concentrations between CuONPs (62.5-250 mg/L) + ϕPB2, it was observed that they could stall and even halt the growth of *R. solanacearum* (Fig. 2H), while at the same concentration, CuONPs alone exhibited weaker inhibition. Remarkably, out of all concentrations evaluated, CuONPs + ϕPB2 at 250 mg/L exhibited the most robust inhibitory effect on *R. solanacearum*. In conclusion, the study suggests that the bactericidal and antibacterial properties of CuONPs + ϕPB2 surpassed those of CuONPs or phage alone. This highlights the potential cross-enhancement of infection capabilities of CuONPs owing to the phage's presence.

The molecular responses of *R. solanacearum* under the stress of CuONPs + ϕPB2

To further investigate the synergetic effects of phage on CuONPs and their bactericidal mechanisms, *R. solanacearum* in the logarithmic phase was treated with DI water, CuONPs (250 mg/L), and CuONPs (250 mg/L) combined with ϕPB2 (1.0×10^6 PFU/mL, 100 μL). Principal component analysis (PCA) for each sample demonstrated a substantial difference among water, CuONPs, and CuONPs + ϕPB2 treatments (SF3A).

For the CuONPs treatment, 91 significantly enriched Gene Ontology (GO) items (Fig. 3A, Table S5) and 7 significantly enriched Kyoto Encyclopedia of Genes

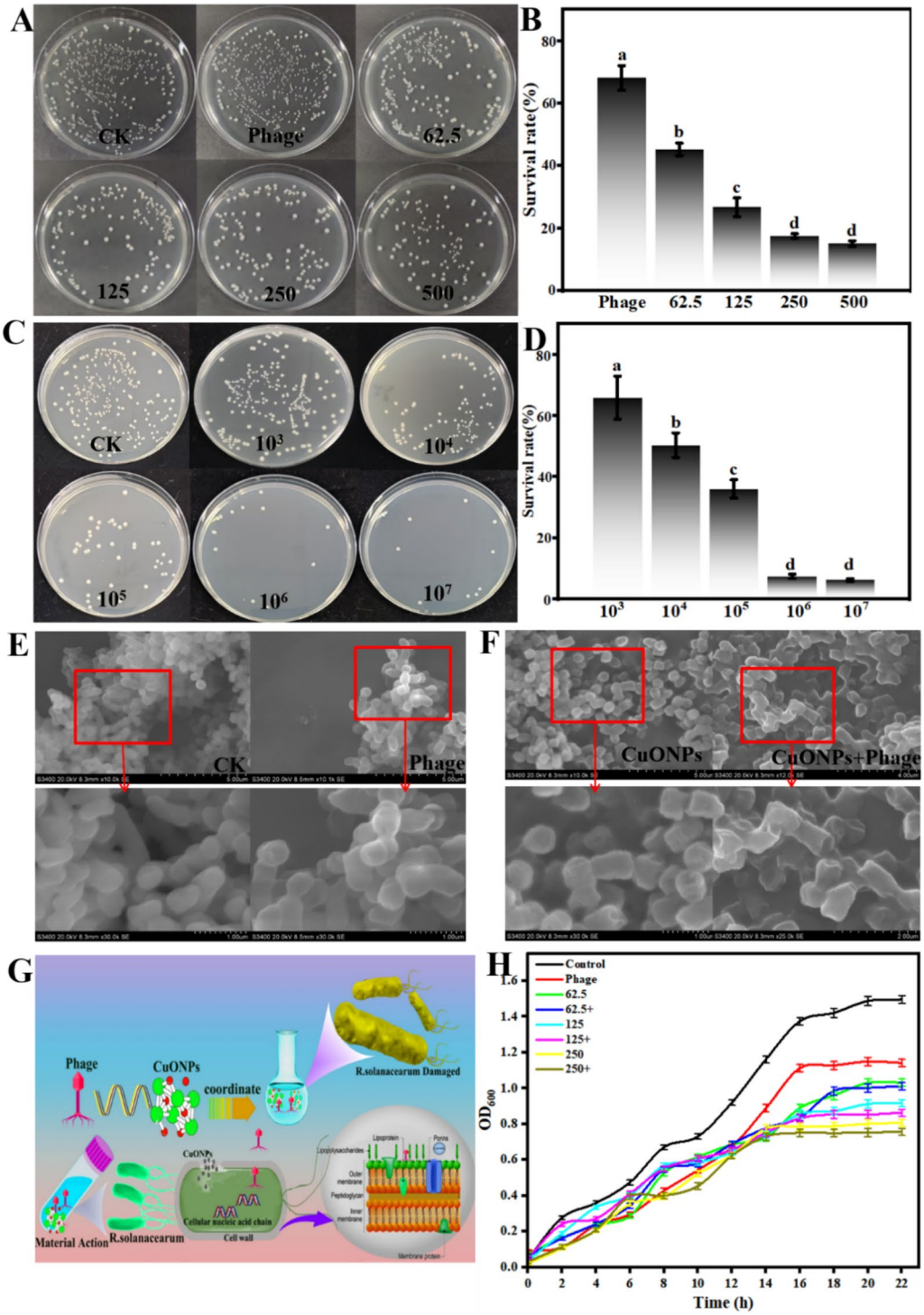

Fig. 2 Antimicrobial activity of CuONPs + φPB2 against *R. solanacearum*. **A** Inhibition effect of different concentrations of CuONPs on *R. solanacearum*. **B** Survival rates of different concentrations of CuONPs on *R. solanacearum*. **C** Effect of different concentrations of phage on CuONPs. **D** Survival rate of different concentrations of phage on CuONPs. **E** SEM images of bacterial wilt (CK, phage and enlarged view). **F** SEM images of *R. solanacearum* (CuONPs, CuONPs + φPB2, and enlarged view). **G** Schematic diagram of CuONPs and phage (φPB2) infection of *R. solanacearum*. **H** Growth curves of *R. solanacearum* after different treatments. Note: "+" indicates that phage are added to the treatments

and Genomes (KEGG) terms for upregulated genes (Fig. 4A) were identified, alongside 217 significantly enriched GO items (Fig. 3B, Table S6) and 8 significantly enriched KEGG terms for downregulated genes (Fig. 4B). Most upregulated genes were associated with the membrane, transporter activity, locomotion, taxis, and chemotaxis (Table S5). The enriched KEGG terms for upregulated genes included "ABC transporters", "two-component system", "bacterial chemotaxis", "biosynthesis of various other secondary metabolites",

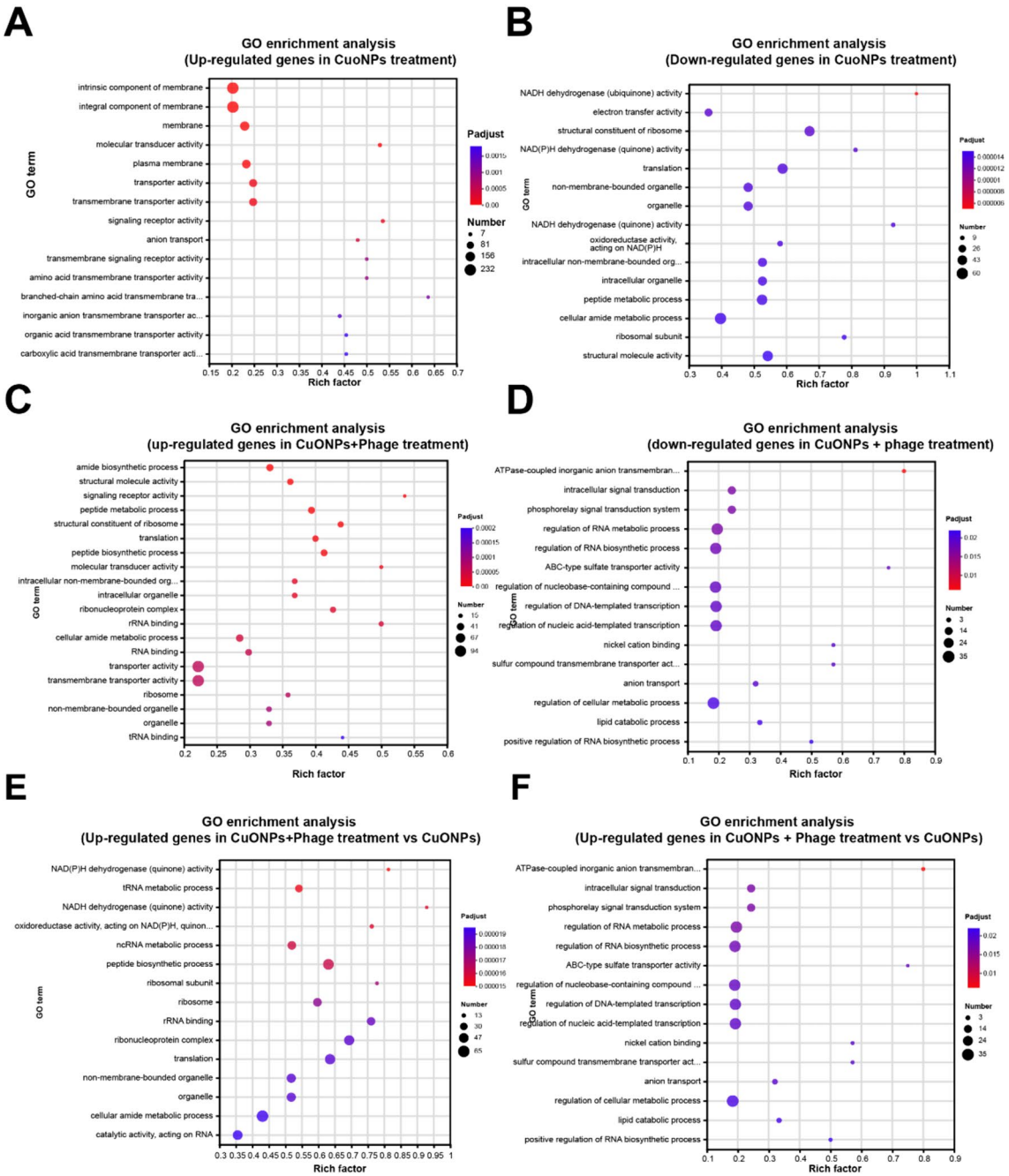

Fig. 3 Significantly enriched GO terms are presented in a bubble diagram for upregulated or downregulated genes in each treatment. The horizontal axis presents the rich factor (the ratio between the number of concerned genes and the number of total transcription genes in the corresponding term). The vertical coordinates indicate the different GO terms. The size of the point shows the concerned gene numbers in the corresponding GO term. The color of each bubble indicates the adjusted *p* value (FDR)

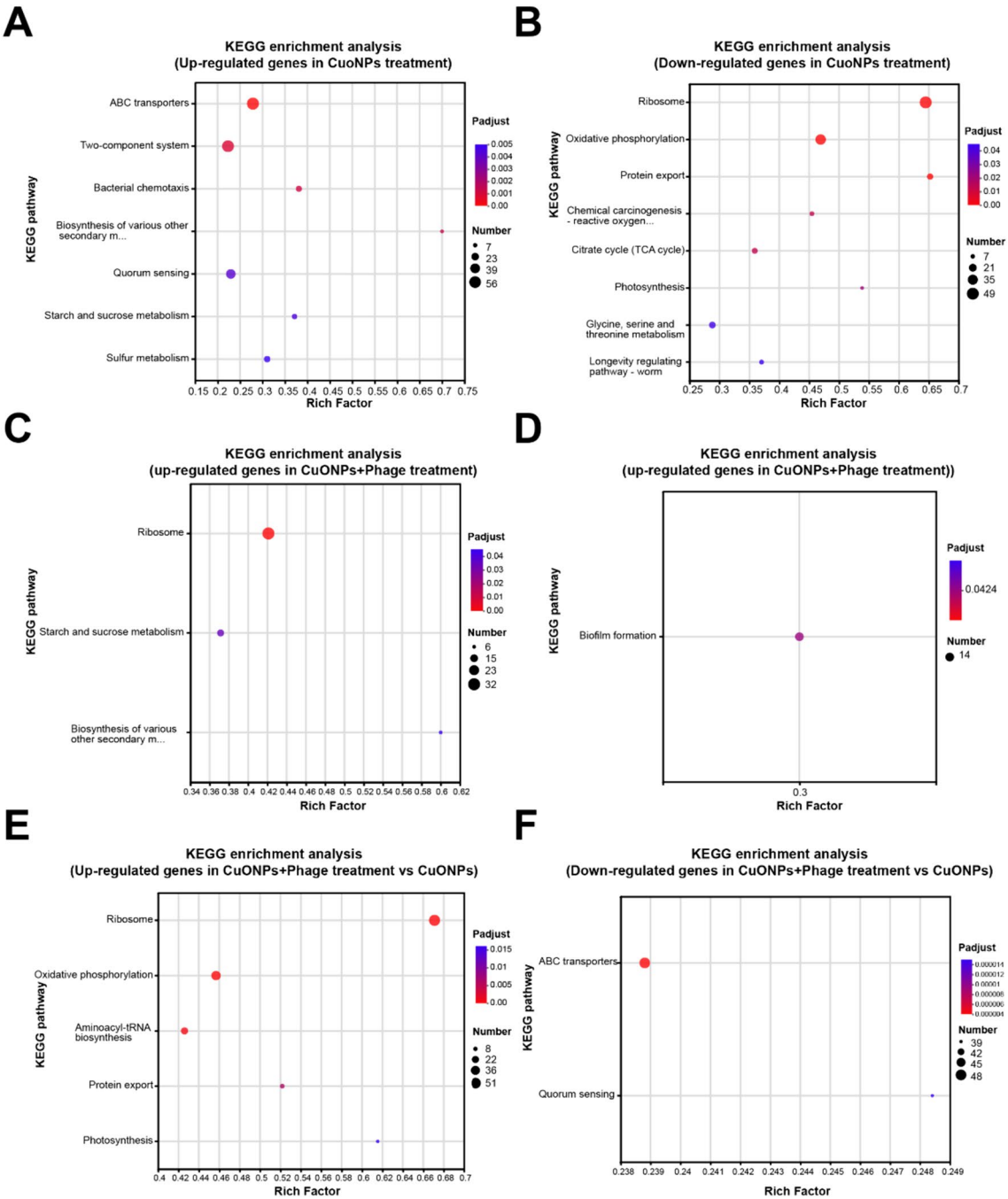

Fig. 4 Significantly enriched KEGG terms are shown in a bubble diagram for upregulated or downregulated genes in each treatment. The horizontal axis shows the rich factor (the ratio between the number of concerned genes and the number of total transcription genes in the corresponding term). The vertical coordinates indicate the different KEGG terms. The size of the point shows the respective gene numbers in the corresponding KEGG term. The color of each bubble indicates the adjusted *p* value (FDR)

"quorum sensing", "starch and sucrose metabolism", and "sulfur metabolism" (Fig. 4A). Conversely, the enriched KEGG terms for downregulated genes were "ribosome", "oxidative phosphorylation", "protein export", "chemical carcinogenesis reactive oxygen species", "citrate cycle (TCA cycle)", "photosynthesis", "glycine, serine and threonine metabolism", and "longevity regulating pathway—worm" (Fig. 3B). These results indicate that CuONPs inhibited processes

related to protein synthesis, respiratory function, and amino acid metabolism.

For the CuONPs + ϕPB2 treatment, 104 significantly enriched GO items from differentially upregulated genes (DUGs) (Fig. 4C, Table S7) and 100 significantly enriched GO items from differentially downregulated genes (DDGs) (Fig. 4D, Table S8) were identified. In contrast to CuONPs treatment, the enriched KEGG terms for upregulated genes from CuONPs + ϕPB2 were "ribosome", "starch and sucrose metabolism", and "biosynthesis of various other secondary metabolites" (Fig. 4C). The only enriched KEGG term for downregulated genes was "biofilm formation" (Fig. 4D). These results implied that CuONPs +ϕPB2 could inhibit the biofilm formation of *R. solanacearum*.

For the comparison between CuONPs + ϕPB2 and CuONPs, most of the upregulated genes were related to molecular function, biological processes, catalytic activity, cellular components, metabolic processes, cellular organelles, and others (Fig. 3E, Table S9). The enriched KEGG terms for upregulated genes were "ribosome", "oxidative phosphorylation", "aminoacyl-tRNA biosynthesis", "protein export", and "photosynthesis" (Fig. 4E). These results implied that phage may stimulate protein synthesis for virus particle assembly, which is different from CuONPs treatment. Most of the downregulated genes were related to the regulation of cellular processes, regulation of metabolic processes, regulation of nitrogen compound metabolic processes, regulation of cellular biosynthetic processes, regulation of gene expression and others (Fig. 3F, Table S10). The enriched KEGG terms for downregulated genes were "ABC transporters" and "quorum sensing" (Fig. 4F). These results implied that both "ABC transporters" and "quorum sensing" were more inhibited by CuONPs + ϕPB2 than by CuONPs. All these different gene expressions explained that why CuONPs + ϕPB2 has higher toxicity than CuONPs on *R. solanacearum*. These results showed that CuONPs + ϕPB2 has higher inhibition on the regulation of cellular processes, regulation of metabolic processes, regulation of nitrogen compound metabolic processes, regulation of cellular biosynthetic processes, regulation of gene expression, "ABC transporters", "quorum sensing", and so on. All these results supported that ϕPB2 could enhance the toxicity of CuONPs through influencing the "ABC transporters" and "quorum sensing", metabolic processes and cellular biosynthetic processes of *R. solanacearum*.

Antibacterial mechanism

Motility inhibition: This experiment investigated the effect of CuONPs combined with phage on the motility of *R. solanacearum* and confirmed its inhibitory effect on twitching and swimming movements (Fig. 5A, C). The colonies of *R. solanacearum* cells on CPG plate are usually sticky and shiny. However, after infection with CuONPs (250 mg/L) or CuONPs (250 mg/L) +ϕPB2, they become smaller and less sticky. The *R. solanacearum* cells show twitching motility and swimming motility in culture [51]. CuONPs or CuONPs + ϕPB2 affects the motility of *R. solanacearum*. On the CPG plate, uninfected bacterial colonies displayed active twitching movement, with large size and an expanded zona pellucid at the edge. In contrast, bacterial colonies infected by CuONPs or CuONPs + ϕPB2 were smaller in area and exhibited narrow and irregular margin, limiting their outward development. Among the different treatments, CuONPs (250 mg/L) + ϕPB2 had the strongest inhibitory effect on bacterial twitching and swimming motility. In addition, the results demonstrate that treatment with CuONPs (250 mg/L) and ϕPB2 results in inhibition rates of 69.57% and 62.59% for floating and rubbing movements, respectively (Fig. 5B, D).

Biofilm inhibition: Whether phage could enhance the antibacterial activity of CuONPs was investigated further (Fig. 5E). The growth of biofilms was inhibited to varying degrees by CuONPs +ϕPB2. Biofilm formation was observed to gradually decrease as a result of the treatment. When compared with the control group (CK), it was found that CuONPs (250 mg/L) significantly reduced bacterial biofilm formation after 24 h. Moreover, the combination of CuONPs (250 mg/L) + ϕPB2 exhibited a higher inhibitory effect on the biofilm formation of *R. solanacearum*, demonstrating a more significant difference compared to the control group. Research has shown that the biofilm formation rate of *E. coli* AB1157 was significantly reduced after AgNPs treatment [49].

ϕPB2 promotes ROS activation induced by CuONPs: The effect of CuONPs + ϕPB2 on the oxidative stress response of *R. solanacearum* was investigated in this experiment (Fig. 5F). The ROS levels gradually increased among CK, ϕPB2, CuONPs (250 mg/L), and CuONPs (250 mg/L) + ϕPB2. Consequently, under the conditions of CuONPs + ϕPB2 treatment, the production of intracellular hydroxyl radicals (•OH) in *R. solanacearum* significantly increased. This indicates that ϕPB2 enhances CuONPs to cause severe oxidative damage to *R. solanacearum*.

Cell membrane permeability and protein leakage analysis: The NPN uptake assay was used to evaluate the effect of exposure to phage and CuONPs on the permeability of the outer membrane of *R. solanacearum* cells [52]. The fluorescence intensity of NPN gradually increased with the effect of CK, ϕPB2, CuONPs, and CuONPs +ϕPB2 in different treatments on *R.*

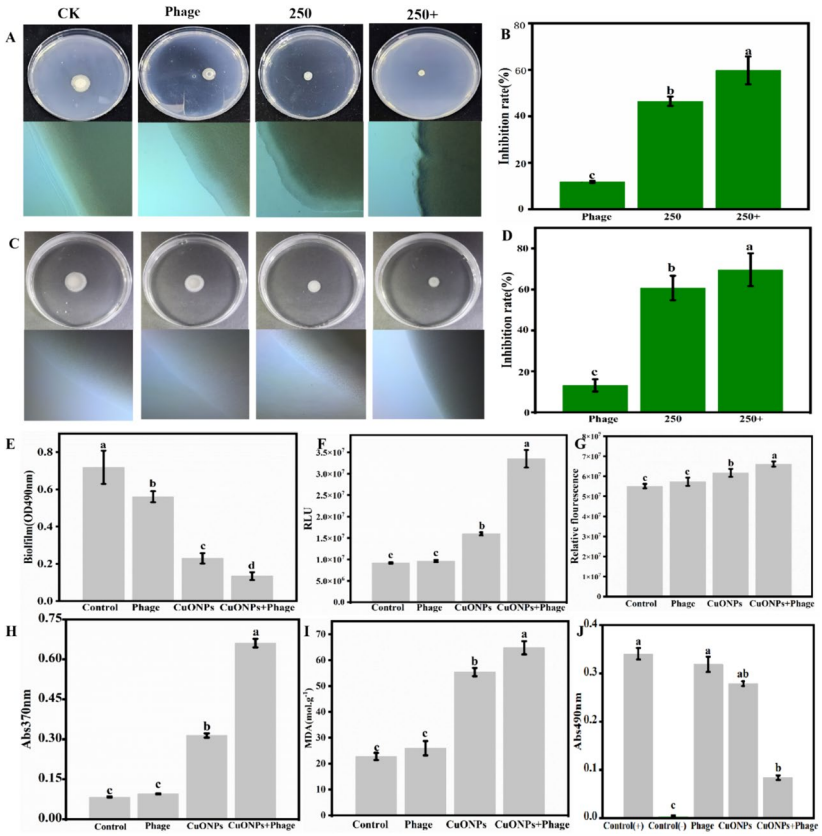

Fig. 5 Effects of different treatments on *R. solanacearum*. **A** Optical microscope map of twitching motility (CK, φPB2, CuONPs (250 mg/L), CuONPs (250 mg/L) + φPB2). **B** Optical microscope map of swarming motility (CK, φPB2, CuONPs (CuONPs (250 mg/L), CuONPs (250 mg/L) + φPB2). **C** The antibacterial rate of twitching motility. **D** The antibacterial rate of swarming motility. **E** Effect of CuONPs and CuONPs + phage on the biofilm formation of *R. solanacearum*. **F** ROS. **G** Cell permeability. **H** Protein leakage of *R. solanacearum* after different treatments. **I** MDA. **J** Cellular respiration chain dehydrogenase. The error bars in the histogram are standard deviations, and lowercase letters a, b, etc., indicate $p < 0.05$

solanacearum (Fig. 5G). Among that, the maximum fluorescence intensity occurred in the CuONPs + ϕPB2 group. This clearly indicates that the permeability of the outer membrane of *R. solanacearum* gradually increased [53].

To confirm bacterial membrane damage, we used the 2,4-dinitrophenylhydrazine colorimetric method as per previous description to evaluate and test protein leakage [54, 55]. The absorbance values at 390 nm after different treatments, 0.083 and 0.095, were only detected in the blank control and phage infection group, respectively. In the group treated with CuONPs at a concentration of 250 mg/L, a detection of 0.314 was observed. The level of protein leakage of CuONPs (250 mg/L) + ϕPB2 was much higher than CuONPs (250 mg/L) group, indicating that the bacterial membrane was more easily destroyed by CuONPs after treatment of ϕPB2 (Fig. 5H).

Determination of MDA and cell chain dehydrogenase: MDA is a product of copper-induced lipid peroxidation. In this study, the TBA method was used to determine the MDA content to determine the degree of lipid peroxidation of nanomaterials [55, 56], and the results are presented in Fig. 5I. The MDA content produced by the blank control group was relatively low, indicating a weak degree of lipid peroxidation. However, after different treatments (CK, ϕPB2, CuONPs (250 mg/L), CuONPs (250 mg/L) + ϕPB2), the MDA content increased, indicating that the degree of bacterial lipid peroxidation increased.

The bacteria were treated with iodonitrotetrazolium violet and different samples, and the enzyme activity of their respiratory chain dehydrogenase was studied (Fig. 5J). The absorbance values at 490 nm after different treatments (Control (+), Control (−), ϕPB2, CuONPs (250 mg/L), CuONPs (250 mg/L) + ϕPB2) were 0.341, 0.004, 0.319, 0.279, and 0.084, respectively. Other treatments inhibited the enzyme activity to varying degrees

compared to the enzyme activity of living cells. Among these treatments, 250 mg/L CuONPs + ϕPB2 exhibited better inhibitory effects, reflecting the experimental results of their high antibacterial rate. The inactivation of dehydrogenase in the respiratory chain of cells may be due to the destruction of the barrier of the cell membrane by CuONPs (250 mg/L) + ϕPB2, thereby inhibiting the respiratory ability of the bacteria.

Bacterial wilt control and plant growth

Pot experiment was conducted to further investigate whether CuONPs + ϕPB2 acts as an antibacterial agent that could be used to protect tobacco plants from bacterial wilt. As shown in Fig. 6A, B, after root irrigation treatment with CuONPs + ϕPB2, the disease index of bacterial wilt was significantly reduced compared to that of the phage and CuONPs group. Then the relative control effects of phage (ϕPB2), CuONPs (250 mg/L), and

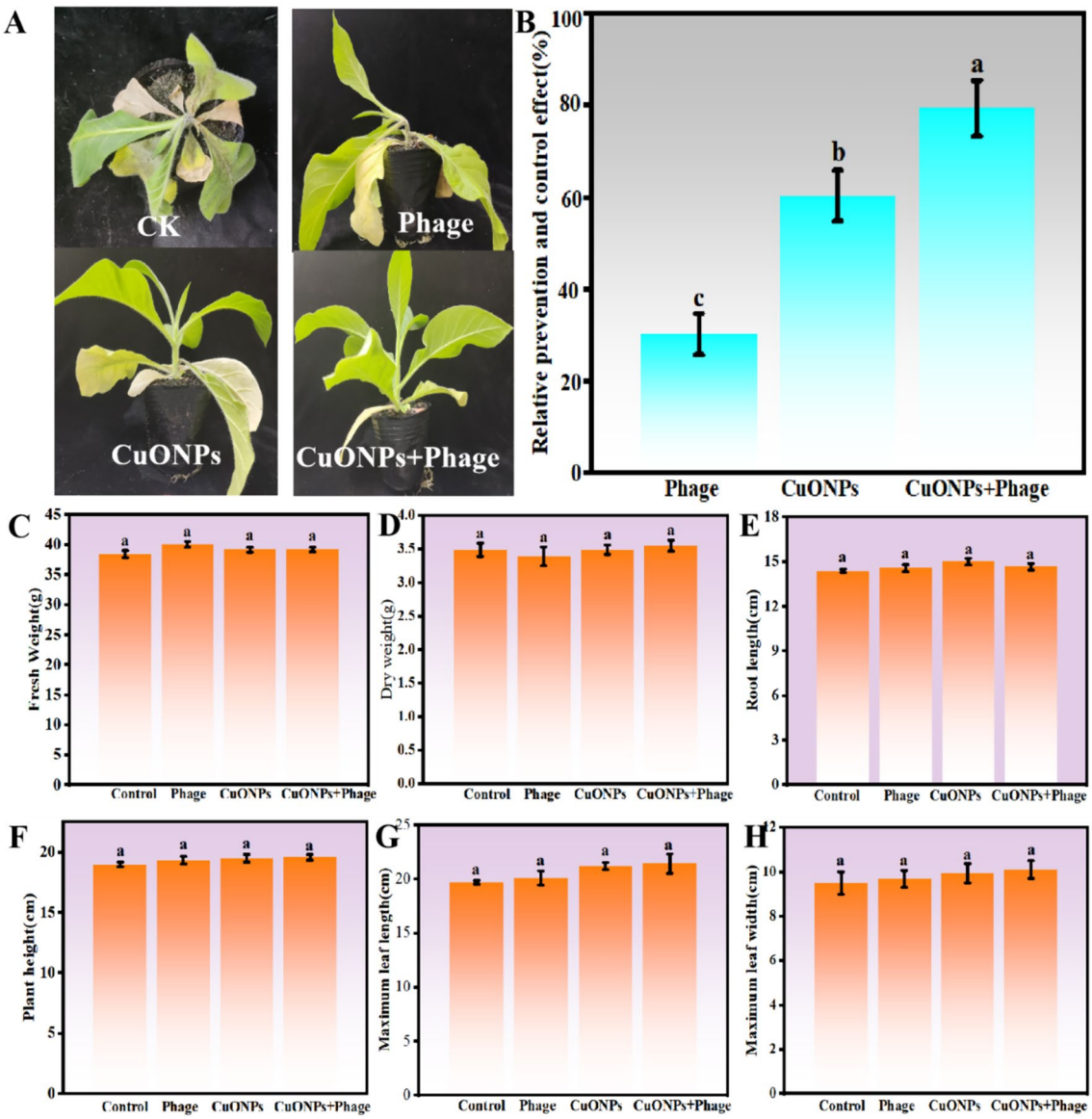

Fig. 6 Effects of CuONPs on tobacco bacterial wilt and seedling growth. **A** The incidence of tobacco bacterial wilt under different treatments. **B** Relative control effects of different treatments on tobacco bacterial wilt disease. **C** Fresh weight. **D** Dry weight. **E** Root length. **F** Plant height. **G** Maximum leaf length. **H** Maximum leaf width. The error bars in the histogram are standard deviations, and lowercase letters a, b, etc., indicate $p < 0.05$

CuONPs (250 mg/L) + ϕPB2 treatment on bacterial wilt disease were 30.16%, 60.32%, and 79.1%, respectively. The disease index of the control plant was greater than that of the bacteria treated with CuONPs, or the disease index treated with phage (ϕPB2). From Fig. 6C–H, after 30 days of treatment growth, there was no significant difference in the growth of tobacco seedlings between different treatments and the control, indicating that phage or CuONPs have no toxic effect on tobacco growth. While studying the antibacterial properties of nanomaterials, it is also necessary to consider their safety effects on plants, the environment, and humans [56]. Cu is an essential trace element for plant metabolism and is involved in different biochemical pathways, including oxygen transport and gene expression activation [57]. Therefore, at this concentration (250 mg/L), the unique antibacterial activity of CuONPs + ϕPB2 may control bacterial wilt. These data reveal that CuONPs + ϕPB2 have broad antibacterial prospects in combating plant pathogens and can serve as a new tool in plant prevention and control.

Discussion

In this study, CuONPs + phage was utilized as a potent "nano microbial agent" for controlling *R. solanacearum* pathogen. Initially, CuONPs were synthesized from orange peel, and subsequently, its high toxicity toward the pathogen was confirmed through antibacterial activity testing and antibacterial mechanism studies. Moreover, CuONPs + phage exhibited inhibitory effects on motility, MDA, and biofilm formation of *R. solanacearum*. We investigated the ultrastructural morphology and gene expression changes to understand the toxicity mechanism of CuONPs + phage on *R. solanacearum*. The results indicated that the CuONPs + phage treatment disrupted the cell membrane system and inhibited various metabolic processes genes of *R. solanacearum*. Moreover, genes of *R. solanacearum* about oxidative stress were upregulated under CuONPs + phage than treatment with CuONPs alone. The inhibitory effect on biofilm and motility may influence the transcriptional expression of motility-related genes in *R. solanacearum*. Previously reported research has highlighted the ability of CuONPs to inhibit the nutritional and reproductive growth of *R. solanacearum*. Given this, it is logical to hypothesize that the combination of CuONPs and phage could lead to increased toxicity against *R. solanacearum*.

To comprehensively assess the impact of CuONPs and phage on various aspects of *R. solanacearum*, transcriptional analysis was carried out. The results indicated that the combination induced oxidative stress and endoplasmic reticulum stress, while also affected cell membrane integrity, signal transduction, transporter protein activity, and metabolic pathways in *R. solanacearum* [58]. The results of upregulated gene GO enrichment analysis (Table S7) indicate that the CuONPs and phage combination induces oxidative stress in *R. solanacearum*. Furthermore, the findings from upregulated gene KEGG enrichment analysis (Fig. 4D, Table S7) demonstrate the induction of endoplasmic reticulum stress by CuONPs and phage in *R. solanacearum*. Conversely, downregulated gene GO enrichment analysis (Table S5) reveals that the cell membrane integrity, signal transduction, and transporter protein activity of *R. solanacearum* are all affected by CuONPs and phage. In addition, the results of downregulated gene KEGG enrichment analysis (Fig. 4E, Table S7) suggest that the metabolic pathways in *R. solanacearum* are partially inhibited by the combination of CuONPs and phage. Ultrastructure observation revealed enhanced cellular damage, including membrane rupture, cytoplasm leakage, thinning of the cell wall, reduced cytoplasm volume, and degradation of intracellular organelles. Notable changes included detachment of the cell membrane from the cell wall, depletion of cytoplasmic matrix and several cytoplasmic organelles, potentially leading to cell death. The anti-biofilm activity is attributed to the release of Cu^{2+} from CuONPs, which integrates onto the surface of bacterial cells, causing cell damage by altering protein structure and enzyme characteristics [59]. This alters hyphal morphology through increased cell permeability. Therefore, it is likely that the primary mechanism of CuONPs + phage in combating *R. solanacearum* lies in its ability to disrupt the cell membrane. Disruption of the cell membrane is a common strategy employed by many antimicrobial agents.

In addition, various antibacterial materials can inhibit biofilm formation, leading to bacterial death. CuONPs + phage disrupts the equilibrium relationship in *R. solanacearum* cells, resulting in metabolic disorders and decreased immune function, thus damaging the cell biofilm and its function. CuONPs increase cell enzyme activity, thereby enhancing cell permeability and thus affecting cell growth and biofilm development, depending on the physicochemical parameters of the growth medium [60]. AgNPs inactivate bacteria by destroying their cell walls and membranes, disrupting the cell's respiratory chain, reducing ATP synthesis, and decreasing bacterial activity [61, 62]. Moreover, various antibacterial materials can inhibit the formation of biofilms, ultimately leading to bacterial death [63, 64]. The disruption of the cell membrane structure by CuONPs + phage is considered one of its important bactericidal mechanisms.

R. solanacearum is a Gram-negative bacterium with a negative charge that creates an electrostatic attraction to positively charged nanoparticles [65]. Thus, we synthesized green nano copper oxide as a preventive and controlling measure against *R. solanacearum*. Previous

studies have shown that nanomaterials exhibit antibacterial properties, inhibiting bacterial growth at micromolar concentrations [66]. Notably, CH-AgNPs led to a reduced incidence of bacterial wilt in tomatoes [67]. In addition, the application of a specific concentration of LaPO4 nanoparticles significantly reduced the pathogen infection rate by 71.4% compared to the control group, yielding similar results in this study [68]. As depicted in Fig. 6, these results are consistent with previously reported results [49]. CuONPs within the range of 250 μg mL^{-1} were determined to have no adverse effects on plants, further supporting the potential benefits of nanomaterials in agricultural applications.

Conclusion

Overall, this study provides a new method using the combination of nanoparticles and phage as chemical substitutes to achieve optimal synergistic effects for controlling bacterial disease. Biosynthetic CuONPs were prepared from ((CuNO3)2 ·5H2O) and orange peel extract, and characterized by XRD, FTIR, SEM, TEM, and XPS. The antibacterial effect of CuONPs alone, phage alone, and the combination of these two agents against *R. solanacearum* was calculated by measuring bacterial growth curves, MDA, and protein leakage. All these experimental data demonstrated that the combination of CuONPs and ϕPB2 significantly reduced the bacterial growth, increased the cell enzyme activity, inhibited the biofilm formation, and intensified the protein leakage compared with other treatments. Transcription analysis revealed that after exposure to CuONPs (250 mg/L) + ϕPB2 for 4 h, cell membrane, transmembrane transporter activity of *R. solanacearum* were stimulated, and the metabolic pathway was downregulated, including molecular function, biological process, cell composition, and metabolic process. Antibacterial mechanism of CuONPs was found to be as a result of wounding cell membrane, hence giving rise to exodus of intracellular content and generation of oxidative reactive oxygen species which invariably inhibited *R. solanacearum* respiration and growth. Therefore, our study indicated that the combination of CuONPs (250 mg/L) and ϕPB2 has better control effect on bacterial infection controlling, and its toxicity mechanism was related with reducing bacterial growth, increasing cell enzyme activity, inhibiting biofilm formation, and intensifying protein leakage. The research results indicated that CuONPs + ϕPB2 can both inhibit the growth of *R. solanacearum* and cause fatal damage. In addition, bacterial cell motility and biofilm formation were inhibited, greatly weakening the virulence of bacteria in the host plant.

Supplementary Information

The online version contains supplementary material available at https://doi.org/10.1186/s40538-024-00630-9.

Additional file 1.
Additional file 2.
Additional file 3.
Additional file 4.
Additional file 5.
Additional file 6.
Additional file 7.
Additional file 8.
Additional file 9.
Additional file 10.
Additional file 11.

Author contributions

Hongbao Zhang, Lin Cai conceived the idea, wrote the manuscript, and revised the manuscript. Lin Cai, Liuti Cai, and Dong Zhou supervised the project and contributed significantly to analysis. Kai Yaun, Zhongwei Liu, Wu Cai, Cheng Rao, and Siang Chen provided experimental space and technical assistance. Hongbao Zhang and Maoyang Ran performed the experiments. Hongbao Zhang analyzed the data and charted the tables and figures.

Funding

This work was supported by the Guizhou Science and Technology Plan Project (ZK[2023]-096), the Major Green Prevention and Control projects from China National Tobacco Corporation (110202101045(LS-05)), the science and technology projects of Guiyang Tobacco Company of Guizhou Province (2021-04), Guizhou University Natural Science Special Post Special Fund (2021-42), China Tobacco Sichuan Industrial Co., LTD(10202317BA500).

Availability of data and materials

No datasets were generated or analyzed during the current study.

Declarations

Ethics approval and consent to participate

Not applicable.

Consent for publication

Not applicable.

Competing interests

The authors declare no competing interests.

Author details

[1]College of Tobacco Science of Guizhou University/Guizhou Key Laboratory for Tobacco Quality/Key Laboratory of Plant Resource Conservation and Germplasm Innovation in Mountainous Region (Ministry of Education), Institute of Agro- Bioengineering, Guiyang 550025, China. [2]Guizhou Tobacco Science Research Institute, Guiyang 550000, China. [3]Sichuan China Tobacco Industry Co., LTD, Chengdu 610101, China. [4]Guizhou Tobacco Company Guiyang City Company, Guiyang 550000, China.

Received: 13 March 2024 Accepted: 22 July 2024
Published online: 03 August 2024

References

1. Shukla PS, Mantin EG, Adil M, et al. Ascophyllum nodosum based bio stimulants: sustainable applications in agriculture for the stimulation of

plant growth, stress tolerance, and disease management. Front Plant Sci. 2019. https://doi.org/10.3389/fpls.2019.00655.
2. Secretariat I, Gullino ML, Albajes R, et al. Scientific review of the impact of climate change on plant pests. 2021. https://doi.org/10.4060/cb4769en.
3. Oerke EC. Crop losses to pests. J Agricu Sci. 2005;144:31–43. https://doi.org/10.1017/S0021859605005708.
4. Savary S, Ficke A, Aubertot JN, et al. Crop losses due to diseases and their implications for global food production losses and food security. Food Sec. 2012;4(4):519–37. https://doi.org/10.1007/s12571-012-0200-5.
5. Mansfield J, Genin S, Magori S, et al. Top 10 plant pathogenic bacteria in molecular plant pathology. Mol Plant Pathol. 2012;13(6):614–29. https://doi.org/10.1111/j.1364-3703.2012.00804.x.
6. Yabuuchi K, Yano HN. Transfer of two Burkholderia and an Alcaligenes species to Ralstoniagen. Nov.: Proposal of Ralstonia pickettii (Ralston, Palleroni and Doudoroff 1973) comb. Nov., Ralstonia solanacearum (Smith 1896) comb. Nov. and Ralstonia eutropha (Davis 1969) comb. Nov. Microbiol Immunol. 1995. https://doi.org/10.1111/j.1348-0421.1995.tb03275.x.
7. Stephane G. Molecular traits controlling host range and adaptation to plants in *Ralstonia solanacearum*. NEW Phytol. 2010;187(4):920–8. https://doi.org/10.1111/j.1469-8137.2010.03397.x.
8. Wang X, Liu X, Han H. Evaluation of antibacterial effects of carbon nanomaterials against copper resistant *Ralstonia solanacearum*. Colloids Surf B Biointerfaces. 2013;103:136–42.
9. Hosseinzadeh S, Shams-Bakhsh M, Hosseinzadeh E. Effects of sub-bactericidal concentration of plant essential oils on pathogenicity factors of *Ralstonia solanacearum*. Arch Phytopathology Plant Prot. 2013;46:643–55.
10. Peeters A, Guidot F, Vailleau MVa. *Ralstonia solanacearum*, a widespread bacterial plant pathogen in the post genomic era. Mol Plant Pathol. 2013;14(7):651–62. https://doi.org/10.1111/mpp.12038.
11. Drulis-Kawa Z. The in vitro anti-pseudomonal activity of Cu^{2+}, strawberry furanone, gentamicin, and lytic phages alone and in combination: *Pros and Cons*. Int J Mol Sci. 2021. https://doi.org/10.3390/ijms22189830.
12. Colin B, Olivia M, Colin H, et al. Bacteriophages and bacterial plant diseases. Front Microbiol. 2017;8(34):79–290. https://doi.org/10.3389/fmicb.2017.00034.
13. Nion YA, Toyota K. Recent trends in control methods for bacterial wilt diseases caused by *Ralstonia solanacearum*. Microbes Environ. 2015;30(1):1–11. https://doi.org/10.1264/jsme2.ME14144.
14. Abdelfattah AS, Hakim TA, Rezk N, et al. Green synthesis of silver nanoparticles using *Ocimum Basilicum L*. and *Hibiscus Sabdariffa L* extracts and their antibacterial activity in combination with phage zcse6 and sensing properties. J Inorg Organomet Polym Mater. 2022. https://doi.org/10.1007/s10904-022-02234-y.
15. Di Lallo G, Evangelisti M, Mancuso F, et al. Isolation and partial characterization of bacteriophages infecting Pseudomonas *syringae pv. actinidiae*, causal agent of kiwifruit bacterial canker. J Basic Microbiol. 2015;54:1210–21. https://doi.org/10.1002/jobm.201300951.
16. Wei C, Liu J, Maina AN, et al. Developing a bacteriophage cocktail for biocontrol of potato bacterial wilt. Virologica Sinica. 2017. https://doi.org/10.1007/s12250-017-3987-6.
17. Alvarez B, Lopez MM, Biosca EG, et al. Biocontrol of the major plant pathogen *Ralstonia solanacearum* in irrigation water and host plants by novel waterborne lytic bacteriophages. Front Microbiol. 2019;10:2813. https://doi.org/10.3389/fmicb.2019.02813.
18. Tanaka H, Negishi H, Maeda H. Control of tobacco bacterial wilt by an avirulent strain of Pseudomonas solanacearum M4S and its bacteriophage. Ja J Phytopathol. 1990;56(2):243–6. https://doi.org/10.3186/jjphytopath.56.243.
19. Fayez MS, Hakim TA, Agwa MM, et al. Topically applied bacteriophage to control multi-drug resistant Klebsiella pneumoniae infected wound in a rat model. Antibiotics. 2021;10(9):1048. https://doi.org/10.3390/antibiotics10091048.
20. Hawes M, Allen C, Turgeon BG, et al. Root border cells and their role in plant defense. Annu Rev Phytopathol. 2016;54(1):143–61. https://doi.org/10.1146/annurev-phyto-080615-100140.
21. Kreuter J. Nanoparticles—a historical perspective. Int J Pharmaceutics. 2007;331(1):1–10. https://doi.org/10.1016/j.ijpharm.2006.10.021.
22. Nickisch MV, Teschke T, Bioscan BF. Construction of an artificial cell membrane anchor using DARC as a fitting for artificial extracellular functionalities of eukaryotic cells. J Nanobiotechnol. 2012. https://doi.org/10.1186/1477-3155-10-1.
23. Tran TM, MacIntyre A, Hawes M, et al. Escaping underground nets: extracellular dnases degrade plant extracellular traps and contribute to virulence of the plant pathogenic bacterium *Ralstonia solanacearum*. PLOS Pathog. 2016;2(6): e1005686. https://doi.org/10.1371/journal.ppat.1005686.
24. Fatema M, Ummul K, Rahman M, et al. Silver/poly (vinyl alcohol) nanocomposite film prepared using water in oil microemulsion for antibacterial applications. J Colloid Int Sci. 2018;514:648–55. https://doi.org/10.1016/j.jcis.2017.12.084.
25. Rajamani L, Enyi Y, David JY, et al. Recent advances in the development of antimicrobial nanoparticles for combating resistant pathogens. Adv Healthcare Materi. 2018;7: e1701400. https://doi.org/10.1002/adhm.201701400.
26. Mahapatra O, Bhagat M, Gopalakrishnan C, et al. Ultrafine dispersed CuO nanoparticles and their antibacterial activity. J Exp Nanosci. 2008. https://doi.org/10.1080/17458080802395460.
27. Chen J, Li S, Luo J, et al. Enhancement of the antibacterial activity of silver nanoparticles against phytopathogenic bacterium *R. solanacearum* by stabilization. J Nanomateri. 2016. https://doi.org/10.1155/2016/7135852.
28. Cai L, Chen J, Liu Z, W, et al. Magnesium oxide nanoparticles: effective agricultural antibacterial agent against *R. solanacearum*. Front Microbiol. 2018. https://doi.org/10.3389/fmicb.2018.00790.
29. Pourmortazavi SM, Taghdiri M, Makari V, et al. Procedure optimization for organism synthesis of silver nanoparticles by aqueous extract of Eucalyptus oleos'. Spectrochem Acta Part A Mol Biomol Spectroscopy. 2015;136:1249–54. https://doi.org/10.1016/j.saa.2014.10.010.
30. Cai L, Ning L, Shen Z, et al. Exploration of bacteriophage resources for *Ralstonia solanacearum* in tobacco. Biol Res. 2018;40(04):339–44. https://doi.org/10.14188/j.ajsh.2018.04.007.
31. Tshireletso P, Ateba CN, Fayemi OE. Spectroscopic and antibacterial properties of CuONPs from orange, lemon, and tangerine peel extracts: potential for combating bacterial resistance. Mol. 2021;26(3):586. https://doi.org/10.3390/molecules26030586.
32. Xia Q, Ran M, Zhou L, Liu Z, Cai L. g-C3N4@CuO electrostatic self-assembly toward *Ralstonia solanacearum*: insights from cytomembrane and motility disruption. Pest Manag Sci. 2024. https://doi.org/10.1002/ps.8047.
33. Kumar A, Pandey AK, Singh SS. A flow cytometric method to assess nanoparticle uptake in bacteria. Cytometry. 2011;79A:707–12.
34. Umrao PD, Kumar V, Kaistha SD. Biocontrol potential of bacteriophage sp1 against bacterial wilt causing *Ralstonia solanacearum* in Solanaceae crops. Egypt J Biol Pest Cont. 2021. https://doi.org/10.1186/s41938-021-00408-3.
35. Hui L, Yumin D, Xiaohui W, Liping S. Chitosan kills bacteria through cell membrane damage. Int J Food Microbiol. 2004;2:147–55. https://doi.org/10.1016/j.ijfoodmicro.2004.01.02.
36. Xu H, Qu F, Xu H, et al. Role of reactive oxygen species in the antibacterial mechanism of silver nanoparticles on Escherichia coli O157:H7. Biometals. 2012;25(1):45–53. https://doi.org/10.1007/s10534-011-9482-x.
37. Tsaturyan V, Poghosyan A, Toczyłowski M, et al. Evaluation of malondialdehyde levels, oxidative stress and host-bacteria interactions: Escherichia coli and salmonella derby. Cells. 2022;11:2989. https://doi.org/10.3390/cells11192989.
38. Anuj SA, Gajera HP, Hirpara DG, et al. Interruption in membrane permeability of drug-resistant Staphylococcus aureus with cationic particles of nano-silver. Eur J Pharm Sci. 2019;127(9):208–16. https://doi.org/10.1016/j.ejps.2018.11.005.
39. Zhang L, Xu JS, Xu J, et al. TssB is essential for virulence and required for type VI secretion system in *Ralstonia solanacearum*. Microbial Pathog. 2014;74:1–7. https://doi.org/10.1016/j.micpath.2014.06.006.
40. Tahir HA, Gu Q, Wu H, et al. Bacillus volatiles adversely affect the physiology and ultra- structure of *Ralstonia solanacearum* and induce systemic resistance in tobacco against bacterial wilt. Sci Rep. 2017. https://doi.org/10.1038/srep40481.
41. Hu W, Li C, Dai J, et al. Antibacterial activity and mechanism of Litsea cubeba essential oil against methicillin-resistant Staphylococcus aureus (MRSA). Ind Crops Prod. 2019;130:34–41. https://doi.org/10.1016/j.indcrop.2018.12.078.

42. Huang X, Xing Y, Jiang H, et al. Nonphytotoxic and pH-responsive ZnO-ZIF-8 loaded with honokiol as a "nanoweapon" effectively controls the soil-borne bacterial pathogen *Ralstonia solanacearum*. J Hazard Mater. 2024;472:0304–3894. https://doi.org/10.1016/j.jhazmat.2024.134502.
43. Mukaihara T, Tamura N, Murata Y, Iwabuchi M. Genetic screening of Hrp type III-related pathogenicity genes controlled by the HrpB transcriptional activator in *Ralstonia solanacearum*. Mol Microbiol. 2004;54(4):863–75. https://doi.org/10.1111/j.1365-2958.2004.04328.x.
44. Cai L, Wei X, Feng H, et al. Antimicrobial mechanisms of g-C3N4 nanosheets against the oomycetes phytophthora capsici: disrupting metabolism and membrane structures and inhibiting vegetative and reproductive growth. J Hazard Mater. 2021;417: 126121. https://doi.org/10.1016/j.jhazmat.2021.126121.
45. Langmead B, Salzberg SL. Fast gapped-read alignment with Bowtie 2. Nat Methods. 2012. https://doi.org/10.1038/nmeth.1923.
46. Li B, Dewey CN. RSEM: accurate transcript quantification from RNA-Seq data with or without a reference genome. BMC Bioinformat. 2011;12(1):323–323. https://doi.org/10.1186/1471-2105-12-323.
47. Xie C, Mao X, Huang J, et al. KOBAS 2.0: a web server for annotation and identification of enriched pathways and diseases. Nucleic Acids Res. 2011. https://doi.org/10.1093/nar/gkr483.
48. Sankar R, Manikandan P, Malarvizhi V, et al. Green synthesis of colloidal copper oxide nanoparticles using Carica papaya and its application in photocatalytic dye degradation. Spectrochim Acta A Mol Biomol Spectrosc. 2014;121:746–750121. https://doi.org/10.1016/j.saa.2013.12.020.
49. Ogunyemi SO, Luo J, Abdallah Y, et al. Copper oxide nanoparticles: an effective suppression tool against bacterial leaf blight of rice and its impacts on plants. Pest Manag Sci. 2024;80:1279–88. https://doi.org/10.1002/ps.7857.
50. Imthiyaz NI. Biosynthesis, characterization and antibacterial activity of copper oxide nanoparticles (CuO NPs) from actinomycetes. Biocatal Agric Biotechnol. 2018;15:56–62.
51. Corral J, Sebastia P, Coll NS, et al. Twitching and swimming motility play a role in *Ralstonia solanacearum* pathogenicity. MSphere. 2020. https://doi.org/10.1128/msphere.00740-19.
52. Helander IM, Mattila-Sandholm T. Permeability barrier of the gram-negative bacterial outer membrane with special reference to nisin. Int J Food Microbiol. 2000;60(2–3):153–61. https://doi.org/10.1016/s0168-1605(00)00307-x.
53. Liu J, Qiao J, Lu ZS, et al. Enhance electron transfer and performance of microbial fuel cells by perforating the cell membrane. Electrochem Commun. 2012;15(1):50–3. https://doi.org/10.1016/j.elecom.2011.11.018.
54. Chatterjee AK, Chakraborty R, Basu T. Mechanism of antibacterial activity of copper nanoparticles. Nanotechnology. 2014;25:135–01. https://doi.org/10.1088/0957-4484/25/13/135101.
55. Draper H Drools, Squires EJ, Mahmoodi H, et al. A comparative evaluation of thiobarbituric acid methods for the determination of malondialdehyde in biological materials. Free Radical Bio. 1993;15(4):353–63. https://doi.org/10.1016/0891-5849(93)90035-S.
56. Kokalj AJ, Hartmann NB, Drobne D, et al. Quality of nanoplastics and microplastics ecotoxicity studies: Refining quality criteria for nanomaterial studies. J Hazard Mater. 2021;41(5):125–751. https://doi.org/10.1016/j.jhazmat.2021.125751.
57. Kadri O, Karmous, Inès, Kharbech O, et al. Cu and CuO Nanoparticles Affected the Germination and the Growth of Barley (*Hordeum vulgare* L.) Seedling. B Environ Contam Tox. 2022;108:585–93. https://doi.org/10.1007/s00128-021-03425-y.
58. Tabasum H, Bhat B, Sheikh BA, et al. Emerging perspectives of plant-derived nanoparticles as effective antimicrobial agents. Inorg Chem Commun. 2022;145:110015. https://doi.org/10.1016/j.inoche.2022.110015.
59. Zielinski ZA, Pratt DA. Lipid Peroxidation: kinetics, mechanisms, and products. J Org Chem. 2017;82(6):2817–25. https://doi.org/10.1021/acs.joc.7b00152.
60. Asharani PV, Low Kah Mun G, Hande MP, et al. Cytotoxicity and genotoxicity of silver nanoparticles in human cells. ACS Nano. 2009;3:279–90. https://doi.org/10.1021/nn800596w.
61. Lok CN, Ho CM, Chen R, et al. Proteomic analysis of the mode of antibacterial action of silver nanoparticles. J Proteome Res. 2006. https://doi.org/10.1021/pr0504079.
62. Mahendra C, Chandra MN, Murali M, et al. Phyto-fabricated ZnO nanoparticles from *Canthium dicoccum* (*L.*) for antimicrobial, anti-tuberculosis and antioxidant activity. Process Biochem. 2020. https://doi.org/10.1016/j.procbio.2019.10.020.
63. Xiao X, Zhu WW, Liu QY, et al. Impairment of biofilm formation by TiO (2) photocatalysis through quorum quenching. Environ Sci Technol. 2016;50(21):11895–902. https://doi.org/10.1021/acs.est.6b03134.
64. Yu Q, Li J, Zhang Y, et al. Inhibition of gold nanoparticles (AuNPs) on pathogenic biofilm formation and invasion to host cells. Sci Rep. 2016. https://doi.org/10.1038/srep26667.
65. Leung Y, Ng AMC, Xu X, Shen Z, Gethings L, Wong MT, et al. Mechanisms of antibacterial activity of MgO: non-ROS mediated toxicity of MgO nanoparticles towards Escherichia coli. Small. 2014;10:1171–83. https://doi.org/10.1002/smll.201302434.
66. Vimbela GV, Ngo SM, Fraze C, Yang L, Stout DA. Antibacterial properties and toxicity from metallic nanomaterials. Int J Nanomed. 2017;12:3941–65. https://doi.org/10.2147/IJN.S134526.
67. Santiago TR, Bonatto CC, Eduardo SG, et al. Green synthesis of silver nanoparticles using tomato leaves extract and their entrapment in chitosan nanoparticles to control bacterial wilt. J Sci Food Agric. 2019;99:4248–59. https://doi.org/10.1002/jsfa.9656.
68. Wang Z, Wang T, Wang C, et al. Lanthanum-based nanomaterials suppress bacterial wilt in tomato: importance of particle morphology and dissolution profiles. Environ Sci Nano. 2023;10:747–60. https://doi.org/10.1039/d2en01040b.

Publisher's Note